Nanoscale

ROYAL SOCIETY OF CHEMISTRY

COMMUNICATION

View Article Online
View Journal | View Issue

Cite this: *Nanoscale*, 2023, **15**, 18581

Received 6th September 2023,
Accepted 26th October 2023

DOI: 10.1039/d3nr04490d

rsc.li/nanoscale

Delivery of graphene oxide nanosheets modulates glutamate release and normalizes amygdala synaptic plasticity to improve anxiety-related behavior†

Elisa Pati, [a] Audrey Franceschi Biagioni, [a] Raffaele Casani,[a] Neus Lozano, [b] Kostas Kostarelos, [b,c] Giada Cellot *[a] and Laura Ballerini *[a]

Graphene oxide nanosheets (GO) were reported to alter neurobiological processes involving cell membrane dynamics. GO ability to reversibly downregulate specifically glutamatergic synapses underpins their potential in future neurotherapeutic developments. Aberrant glutamate plasticity contributes to stress-related psychopathology and drugs which target dysregulated glutamate represent promising treatments. We find that in a rat model of post-traumatic stress disorder (PTSD), a single injection of GO to the lateral amygdala following the stressful event induced PTSD-related behavior remission and reduced dendritic spine densities. We explored from a mechanistic perspective how GO could impair glutamate synaptic plasticity. By simultaneous patch clamp pair recordings of unitary synaptic currents, live-imaging of presynaptic vesicle release and confocal microscopy, we report that GO nanosheets altered the probability of release enhancing the extinction of synaptic plasticity in the amygdala. These findings show that the modulation of presynaptic glutamate release might represent an unexplored target for (nano)pharmacological interventions of stress-related disorders.

1. Introduction

By virtue of their nanoscale dimensionality, combined with specific chemical–physical properties[1–4] engineered graphene-based nanomaterials (GBNs) are increasingly explored as advanced drug delivery platforms, or as components of interfacing devices to treat central nervous system (CNS) diseases.[5–8] Among GBNs, small graphene oxide (GO) nanosheets (s-GO, <500 nm lateral dimension) have been shown to target CNS glutamatergic synapses inducing a reversible reduction in excitatory neurotransmission in the rat hippocampus *in vitro* and *in vivo*.[9] Furthermore, the same nanosheets have been reported to enable the experimental modulation of spinal circuit activity and correlated swimming behavior in the zebrafish.[10] This neuro-modulatory feature of s-GO was recently translated in a proof-of-concept (neuro)pathological context, to prevent the consolidation of early alterations in glutamatergic transmission responsible for long-term pathological behaviors, within the framework of post-traumatic stress disorder (PTSD) and amygdala synaptic plasticity.[11]

PTSD belongs to the spectrum of anxiety diseases and features a dysfunctional long-term potentiation (LTP) in the lateral amygdala (LA) nucleus, causing hyperactivity of glutamatergic synapses[12–14] correlated with long-lasting anxiety-related behaviours.[15,16] We previously reported that s-GO nanosheet suspensions stereotaxically injected into the LA to target glutamatergic synapses, were able to prevent efficiently PTSD-related behavioral responses within 48 hours post-injection.[11] The direct interference of the nanomaterial with the presynaptic site of synapses was hypothesised.[9,11] However, the mechanism(s) through which s-GO nanosheets block glutamatergic synapses preventing the build-up of potentiated activity in the amygdala circuits and whether such a block is sustaining a long-lasting normalization of pathological behavior, leading to PTSD remission, have not been elucidated.

In the current work, the amygdala synaptic enhancement (*i.e.* LTP[12–14]), which follows traumatic stress in a rat behavioral model of PTSD, was treated with a single s-GO injection directly in the LA. s-GO downregulated long-lasting anxiety related behaviors, and such an effect outlasted the nanomaterial presence in the CNS. We further explored with a series of mechanistic investigations the interactions among

[a]*Neuroscience Area, International School for Advanced Studies (SISSA/ISAS), 34136 Trieste, Italy. E-mail: cellot@sissa.it, laura.ballerini@sissa.it*
[b]*Nanomedicine Lab Catalan Institute of Nanoscience and Nanotechnology (ICN2), CSIC and BIST, Campus UAB, Bellaterra, 08193 Barcelona, Spain*
[c]*Nanomedicine Lab, and Faculty of Biology, Medicine & Health, The National Graphene Institute, University of Manchester, Manchester, M13 9PL, UK*

†Electronic supplementary information (ESI) available: Materials and methods. Fig. S1: Characterization of s-GO sheets. Fig. S2: s-GO does not alter the amygdala synapses in control conditions. Fig. S3: s-GO does not affect either the activity of postsynaptic glutamatergic receptors or the exogenously applied glutamate. Fig. S4: s-GO and vesicle release dynamics in control amygdala neurons. Fig. S5: s-GO modulatory effect on synaptic release probability is transient. See DOI: https://doi.org/10.1039/d3nr04490d

s-GO and glutamatergic synapses. To dissect s-GO activity at the presynaptic site, we used an *in vitro* model of amygdala circuits where LTP of excitatory synapses can be chemically induced.[11] By combining confocal microscopy and live imaging of amygdala synapses, with patch-clamp simultaneous recordings from pairs of monosynaptically connected neurons, we explored s-GO modulation of vesicle release at the glutamatergic synapses. We additionally showed that LTP-induced changes in synaptic morphological and functional features were impaired by s-GO. Based on our results, we suggest that s-GO, by reducing the releasable vesicle pool at glutamatergic amygdala synapses, was able to efficiently block pathological LTP.

2. Results

2.1 *In vivo* long-lasting normalization of PTSD-related behavior upon single s-GO injection in the LA

Following stressful events, LA glutamatergic synapses undergo plastic changes responsible for the storage of aversive memory and such form of LTP sustains the emergence of PTSD. We used a rat behavioral model of PTSD, in which the exposure to the predator odor, by inducing LTP of glutamatergic synapses in LA,[17] causes the behavioral response typical of traumatic disorders.[18] We delivered a single injection of s-GO in the LA, shortly following the stressful event and in the presence of innate fear response, to assess whether targeting glutamatergic synapses[11] could induce a long-lasting impairment of LTP development. Although cleared from the brain tissue within 48 hours[9] we hypothesized that if s-GO was successful in blocking synapse potentiation, it should disrupt long-term aversive memory and long-lasting anxiety-related behaviors.

Rats (n = 20), upon habituation to an apparatus to study contextual fear memory (avoidance box,[19] Fig. 1A and B), were exposed to a collar previously worn (WC) by a cat, or to an unworn collar (UC, control group; sketched in Fig. 1A and B). Compared to the UC group, WC rats showed immediately a significant innate fear response characterized by an increase ($t(10)$ = 8.54, p = 0.0001; Fig. 1C) in the head out behavior, which allows maintaining a protected position when scanning the environment.[11] The day after, rats were submitted to a stereotaxic surgery to position a cannula in the LA, through which, 4 days later, 0.5 μL of s-GO (50 μg mL^{-1}) or of the vehicle (saline) were microinjected.[11] The nanomaterial used in this work was synthesized according to already reported protocols and was characterized extensively in our previous publications.[9–11,20] A characterization of the specific batch of GO nanosheets used here is reported in ESI Fig. 1.†

Different from our previous investigation,[11] we explored long-lasting fear- and anxiety-related behaviors upon rat re-exposure to the context (in the absence of the collars) 8 days after the odor exposure, namely 4 days after s-GO or saline injections. WC animals, when saline treated, after 8 days still presented a significant increase in head out behavior respect to UC exposed ones (saline or s-GO treated ($F(1, 5)$ = 11.76, p = 0.0036) and ($F(1, 5)$ = 11.76, p = 0.0113), respectively), while when WC rats were treated by s-GO the head out defensive behavior was reverted ($F(1, 5)$ = 24.71, p = 0.0187; Fig. 1C). We tested long-term anxiety-related response by the elevated plus maze (EPM, Fig. 1D), an apparatus composed of 4 interconnected arms, two open and two closed, used to measure anxiety-like responses.[21] WC rats, treated with saline, exhibited a statistically significant decrease ($F(1, 5)$ = 9.219, p = 0.0289; Fig. 1E) in the time spent in the EPM open (aversive) arms when compared to UC (saline or s-GO treated) groups, a behavior indicative for long-lasting PTSD. Differently, s-GO microinjection into LA increased ($F(1, 5)$ = 12.79, p = 0.0159) the time spent in the EPM open arms by WC animals, when compared to WC saline treated group (Fig. 1E). Open field (OF) analysis of locomotor activity showed no alterations in animal performance in UC or WC, saline or s-GO treated ($p > 0.05$; Fig. 1F and G).

After the behavioral experiments, rodents were sacrificed, and brains were stained by Golgi-Cox (see Methods). We histologically confirmed the correct targeting of the cannula to the LA (Fig. 1H, as injection needle tracts into the LA between bregma −2.64 mm and −3.96 mm) and quantified LA dendritic spine density (see Methods), whose increase is considered a hallmark of amygdala plasticity associated with fear memory[22] and the development of PTSD.[23,24]

In WC treated with saline the number of dendritic spines per dendrite length (μm) in LA was significantly higher (1.12 ± 0.05) when compared to UC-saline (0.92 ± 0.06, $F(1, 11)$ = 3.925, p = 0.0142) or to UC-s-GO treated groups (0.83 ± 0.08, $F(1, 11)$ = 5.368, p = 0.0014). Notably, WC treated by s-GO did not show the LA increase in dendritic spine density (0.88 ± 0.04, $F(1, 11)$ = 3.69, p = 0.0214, Fig. 1I and J). We conclude that, being the increased dendritic spine protrusions one of the key structural features of LTP, s-GO activity on glutamatergic synapses in LA affected plasticity changes related to PTSD.

2.2 s-GO prevent the expression of LTP-induced synaptic changes in the amygdala

To further determine the mechanism responsible for s-GO blocking of LTP, we performed experiments in amygdala cultured neurons. We addressed by confocal analysis the structural modifications of excitatory synapses following chemical LTP (cLTP) potentiation and whether, when cLTP mechanisms were triggered in the presence of s-GO, such changes were affected by the nanomaterial. Dissociated amygdala cultures underwent to cLTP procedure (30 s exposure to 50 μM of glutamate[11]) in the presence or absence of s-GO (20 μg mL^{-1}, co-applied with glutamate), while controls were exposed to 30 s saline solution (Fig. 2A). All cultures were fixed for immunolabelling 30 minutes after glutamate or saline exposure. Fig. 2B shows representative confocal z-stack reconstructions of triple labelling with antibodies against the neuronal marker β-tubulin III (in blue),[9] against the glutamatergic presynaptic marker VGlut1 (in green)[25] and the glutamatergic postsynaptic marker PSD95 (in red).[26,27]

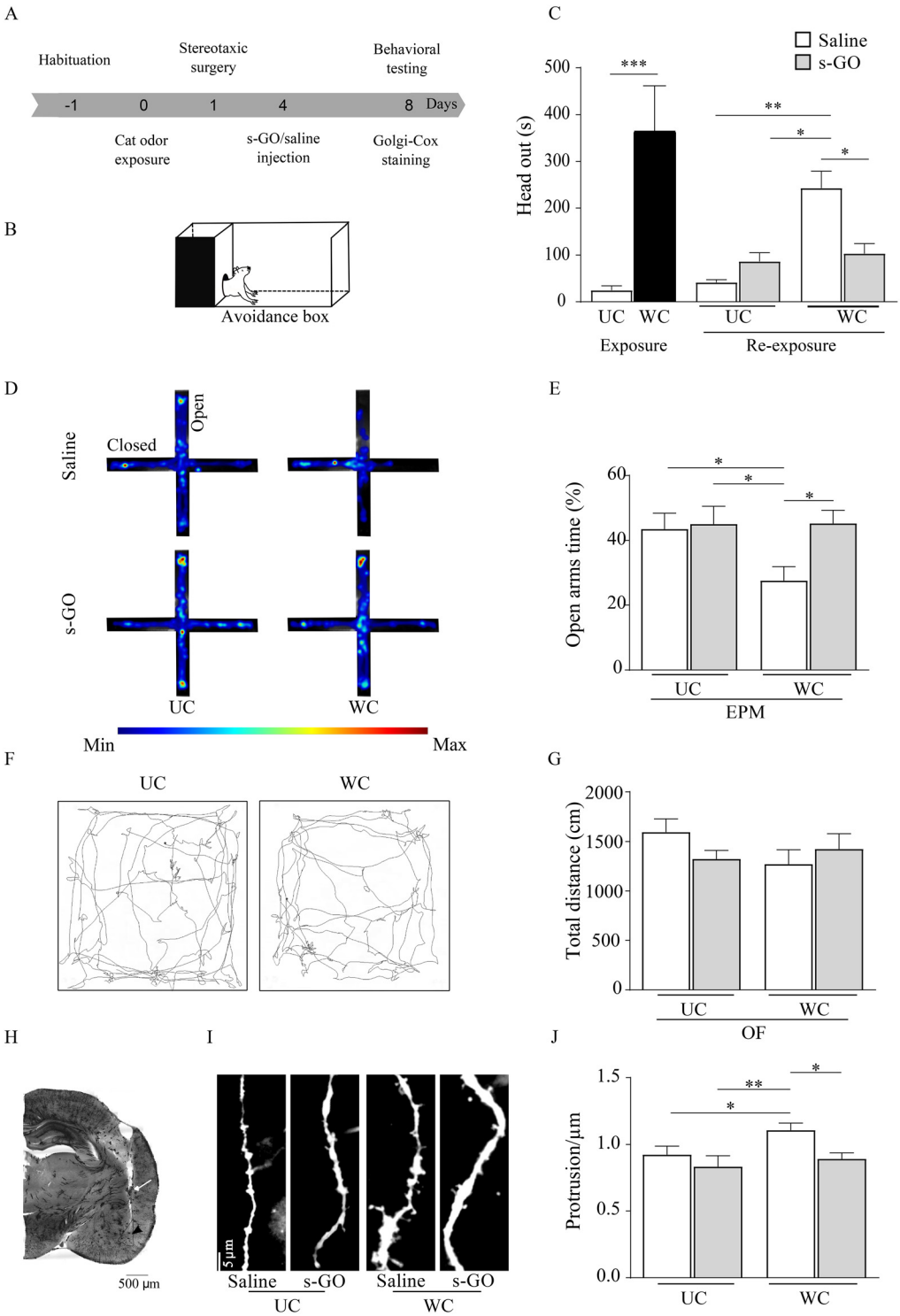

Fig. 1 Fear memory impairment and PTSD-related behavior remission caused by s-GO injected into LA. (A) Schematic representation of the experimental timeline and behavioral testing. (B) Representative image of avoidance box sketching the head out behavior; (C) bar plot summarizing the head out behavioral responses evoked by the exposure to UC or WC and by the re-exposure to the context 4 days after microinjections of saline or s-GO into the LA. (D) Cumulative heat maps of the time spent in the arms of the EPM by UC and WC groups treated with saline or with s-GO. (E) Bar plot showing the time spent in the open arms of EPM apparatus in UC and WC group treated with saline or with s-GO. (F) Illustration of two representative sample tracks from a UC (left) and WC (right) group recorded during the OF test. (G) Bar plot reporting the total distance travelled in the OF apparatus in UC (n = 4) and WC (n = 6) groups, both treated with saline or with s-GO. n = 6 for each group. (H) Photomicrographs of a Golgi-Cox-impregnated coronal section with a representative cannula placement directed to LA. The white arrow indicates the end of the guide cannula, and the black arrow indicates the tip of the microinjection needle. (I) Representative dendritic segments of LA neurons in UC and WC rats treated with saline or with s-GO. (J) Bar plot shows the mean number of spines detected within 40 µm segment of LA dendrites in UC and WC rats. n = 4 per group, n = 12 neurons per group, respectively. ***p < 0.001; **p < 0.01; *p < 0.05.

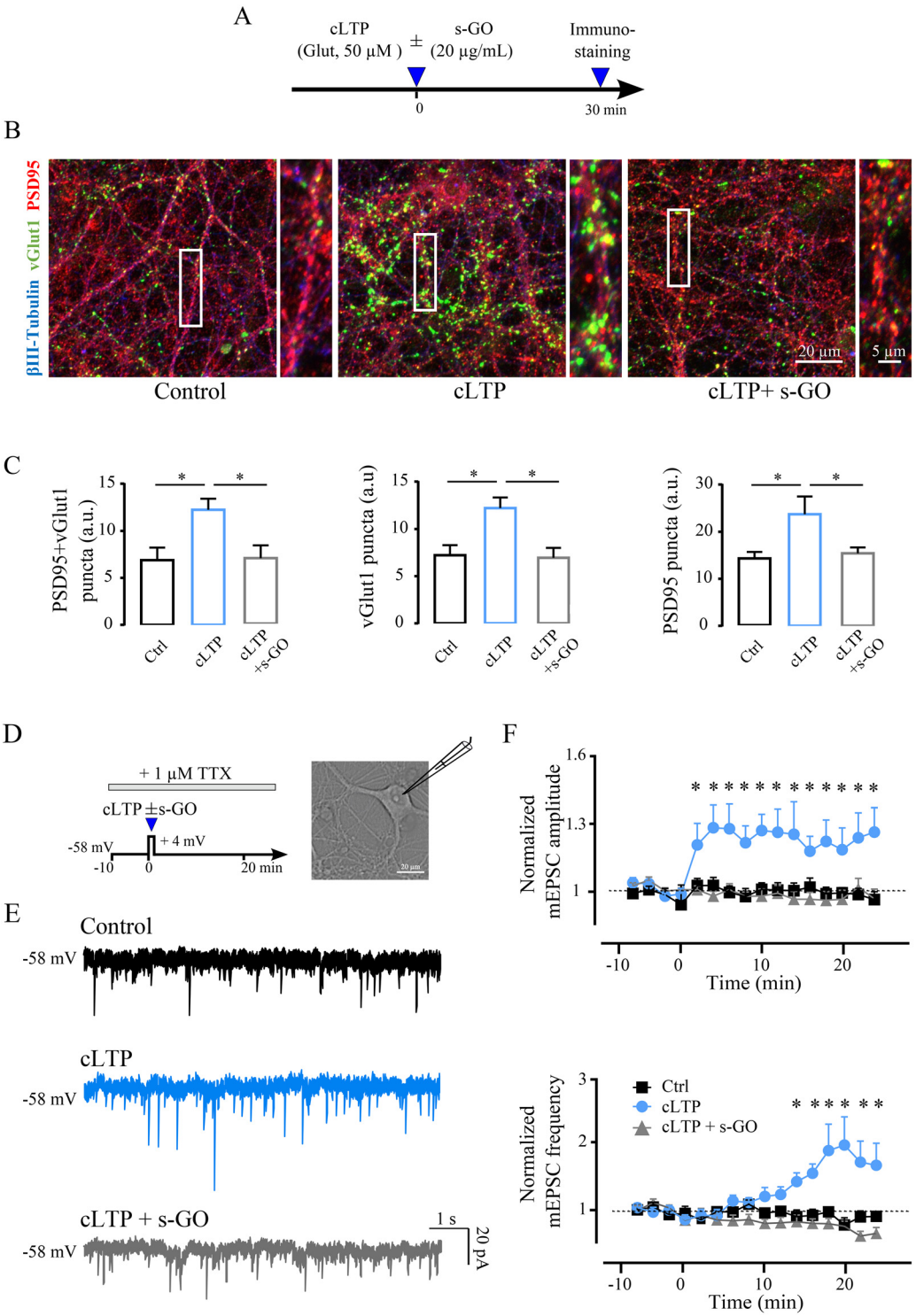

Fig. 2 s-GO prevent cLTP-related structural and functional features in culture. (A) Schematic representation of the experimental setting. Dissociated amygdala cultures (8–12 DIV) were exposed to treatments with saline (control), glutamate (cLTP) or glutamate + s-GO (cLTP + s-GO). (B) Confocal images of neuronal cultures in control, cLTP and cLTP + s-GO labelled for VGlut1 (in green) and PSD95 (in red) and β-tubulin III (blue). Higher magnifications of the highlighted regions (white rectangles) are depicted on the right of each panel. (C) Histograms summarizing PSD95, VGlut1 and PSD95 + VGlut1 puncta densities in the three conditions. (D) Experimental protocol (left) for single-cell voltage clamp recordings, bright field image (right) of a patched neuron. (E) Exemplificative traces of mPSCs detected 20 min after the saline application (30 s, saline, in black), after glutamate (30 s, cLTP, in blue) or glutamate + s-GO (30 s cLTP + s-GO, in grey). (F) Plots showing that s-GO treatment blocked the 24 min long lasting increase in mEPSC amplitude (top), and frequency (bottom) observed in neurons undergone to the LTP induction. *$p < 0.05$.

In β-tubulin III positive cells, we quantified VGlut1 + PSD95 co-localized puncta, indicative for the presence of excitatory synaptic contacts,[28] which were significantly increased 30 min after cLTP when compared to controls (6.9 ± 1.3 a.u. in control and 12.2 ± 1.2 a.u. in cLTP-treated cultures; $p = 0.015$; $n = 20$ fields, 4 cultures each; bar plots in Fig. 2C). Such an increase was not measured when cLTP was induced in the presence (30 s) of s-GO (7.0 ± 1.4 a.u.; cLTP *vs.* cLTP + s-GO $p = 0.015$; Fig. 2C). Similar results were described when analyzing separately VGlut1 puncta and PSD95 puncta in control, cLTP or cLTP + s-GO (bar plots in Fig. 2C). The mere exposure of control amygdala neurons to s-GO (20 μg mL^{-1}, 30 s) did not change significantly co-localized puncta when compared to un-exposed controls (ESI Fig. 2A and B†), suggesting that s-GO prevented LTP-puncta increase specifically blocking functional synaptic potentiation.

Electrophysiological voltage-clamp recordings in the presence of tetrodotoxin (TTX 1 μM)[29] allowed to isolate miniature postsynaptic currents (mPSC; see ESI†); cLTP of mPSCs was induced by coupling glutamate application (50 μM; 30 s) with simultaneous depolarization to +4 mV holding potential of the recorded neuron[30,31] (sketched in Fig. 2D). We monitored (24 min) mPSC frequency and amplitude values after cLTP, induced in the absence ($n = 18$) or in the presence of s-GO ($n = 16$), and in control (*i.e.* neurons depolarized for 30 s without the application of the chemicals; $n = 17$). Fig. 2E depicts sample traces, showing that cLTP treatment (in light blue) at steady state induced an increase in both the frequency (+26%) and amplitude (+60%) of mPSCs respect to the control (in black). When performed in s-GO, cLTP did not potentiate miniature currents amplitude or frequency (in gray, Fig. 2E).

Miniature excitatory postsynaptic currents (mEPSC) were sampled out (see Methods) and their frequency and amplitude values (normalized to baseline) were plotted against time (Fig. 2F). In most neurons (61%) a stable and statistically significant increment in amplitude was detected starting <2 min after cLTP. Normalized mEPSC amplitude at steady state (18–24 min) was 1.00 ± 0.02 in controls and 1.20 ± 0.11 in glutamate treated cells ($p = 0.01$). mEPSC normalized frequency values increased upon cLTP, but with a delay (14 min), reaching significancy at steady state (from 0.88 ± 0.07 in controls to 1.79 ± 0.30 in glutamate treated cells; $p = 0.01$; Fig. 2F). When in the presence of s-GO, cLTP did not potentiate mEPSCs amplitude and frequency (steady state amplitude 0.95 ± 0.04, $p = 0.014$, and frequency 0.77 ± 0.07, $p = 0.011$; Fig. 2F). When s-GO was applied *per se* for 30 s to control cultures, it did not affect mEPSCs (see ESI Fig. 2C and D†). When similarly analyzing miniature inhibitory postsynaptic current (mIPSC; see Methods) we did not detect changes in amplitude or frequency upon both treatments: cLTP (amplitude 0.96 ± 0.04, frequency 0.92 ± 0.16) or cLTP and s-GO (amplitude 0.96 ± 0.04, frequency 0.89 ± 0.08), when compared to control (amplitude 0.98 ± 0.03, frequency 0.91 ± 0.07; all $p > 0.05$).

cLTP reliably induced successful and long-lasting glutamatergic synaptic potentiation in amygdala networks. Both the morphological and functional signatures of potentiation were readily prevented by s-GO when co-applied to glutamate during cLTP induction. We designed the next series of experiments to elucidate the subcellular target of s-GO enabling cLTP block at glutamatergic synapses.

2.3 s-GO acts on the presynaptic terminal of amygdala neurons affecting presynaptic vesicle dynamics

s-GO may target pre-synaptic release at central glutamatergic synapses,[9,10] thus we wondered whether specific and transient impairment of vesicle release could prevent cLTP in the amygdala, and abolish long term neurotransmission changes. We first ruled out s-GO post-synaptic effects, such as glutamate receptors impairment and/or glutamate buffering (*e.g.*, through adsorption). In ESI Fig. 3,† we applied glutamate (50 μM, 30 s) to pharmacologically (1 μM TTX) isolated neurons, and we measured the evoked glutamate receptor-mediated inward currents areas which were not changed by s-GO (20 μg mL^{-1}) co-application (glutamate 13.4 ± 5.1 pA*ms, $n = 12$, and glutamate + s-GO 10.2 ± 6.2 pA*ms; $n = 10$, $p > 0.05$).

We used the fluorescent styryl dye FM1-43 for real-time imaging of vesicles recycling at synaptic terminals[32–34] (Fig. 3A). Presynaptic vesicles in amygdala cultures were loaded with the dye following endocytosis activated by cell depolarization[34] (by 50 mM KCl, 2 min; ESI Fig. 4A;† see Methods). Next, in the presence of TTX, samples were exposed (as in Fig. 2F) to saline (control), to cLTP (50 μM of glutamate for 30 s) and cLTP in the presence of s-GO (20 μg mL^{-1}). In each group, presynaptic vesicle release rate was measured 30 min after treatments by a second KCl application (Fig. 3A), a stimulation condition known to release the *exo-*/*endo*-cycling pool of vesicles.[35] Under these experimental paradigms, the destaining of FM1-43 dye from the presynaptic boutons represents a direct measure of presynaptic release efficacy of the releasable pool of vesicles.[36]

FM1-43 dye loading is not specific for glutamatergic vesicles, therefore we imaged presynaptic terminals of pyramidal neurons, visually identified (bright field) by their morphology[37] (see Methods). cLTP neurons displayed FM1-43 dye unloading characterized by a decay time constant (τ) of 9.6 ± 0.37 s ($n = 200$ terminals) which was significantly faster respect to control unloading τ of 18.5 ± 2.3 ($n = 200$ terminals; $p < 0.0001$; Fig. 2B and C). Co-application of s-GO prevented cLTP increase in FM1-43 destaining, which remained comparable to controls (τ 16.4 ± 1.7 s, $n = 199$ terminals, $p < 0.0001$ for cLTP *vs.* cLTP + s-GO; $n = 5$ series of cultures for each condition, Fig. 3B and C). Baseline bleaching of FM1-43 fluorescence was estimated in the absence of high-K^+ stimulated exocytosis, shown in Fig. 3B (in red). In control cultures, application of s-GO *per se* increased τ when compared to controls (ESI Fig. 4B and C†), supporting the hypothesized s-GO targeting of presynaptic vesicle re-cycling.[9,10] Overall, these results suggested that s-GO by reducing the readily releasable pool, prevented the increase in mobility of synaptic vesicles and the related enhanced probability of release (p_r) featured by cLTP.

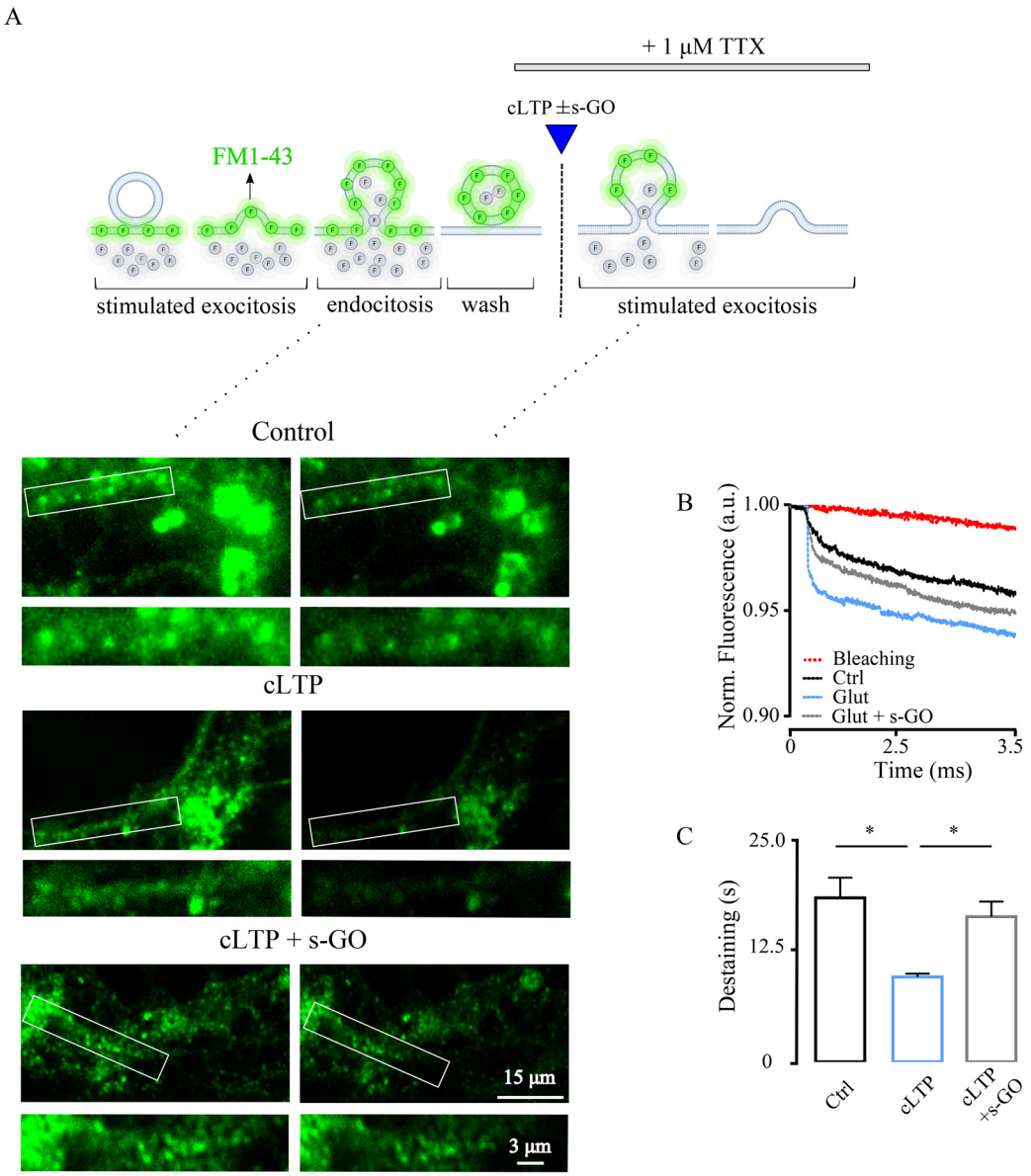

Fig. 3 s-GO affects the presynaptic vesicle release from amygdala neurons. (A) Sketch of the experimental setting (top) of sequential FM1-43 staining and destaining (bottom): fluorescence micrographs of neurite staining with FM1-43 (right) followed by 50 KCl-induced destaining (left) in control, cLTP and cLTP + s-GO conditions. (B) Representative traces of fluorescence decrease upon KCl stimulation in control (black line), cLTP (blue line) and cLTP + s-GO (grey line). In red the fluorescence bleaching after KCl stimulation. Each trace is normalized to the detected maximum fluorescence. (C) The histogram summarizes the decay time constant (τ) of FM1-43 destaining in the three conditions. *$p < 0.05$.

2.4 s-GO reduces the probability of glutamate release is the primary mechanism of LTP block in amygdala synapses

We performed simultaneous electrophysiological recordings from monosynaptically connected pairs of excitatory amygdala neurons, in such a setting pair pulse stimulation protocol allows the direct measure of p_r.[38–41] In each pair, the presynaptic neuron was stimulated in current clamp mode to fire two action potentials at 20 Hz while simultaneously monitoring the voltage clamped postsynaptic cell to assess changes in the amplitude of the two consecutive evoked excitatory postsynaptic currents (eEPSC; in the presence of 10 μM gabazine, see Methods; Fig. 4A). In pair recordings, cLTP induced an increment in the amplitude of first eEPSC (amplitude normalized to pre-treatment values 1.7 ± 0.12) in respect to the control (0.84 ± 0.07; $p = 0.003$) and such an enhancement was not measured in cLTP with s-GO (0.80 ± 0.09; $p = 0.003$, Fig. 4B).

Changes in the pair pulse ratio (PPR), namely the ratio between the second and the first eEPSC peak amplitudes,[41,42] were monitored before (left column, Fig. 4B) and after (right column) the different treatments to report modifications in the p_r, since decreases and increases in PPR are indicative for

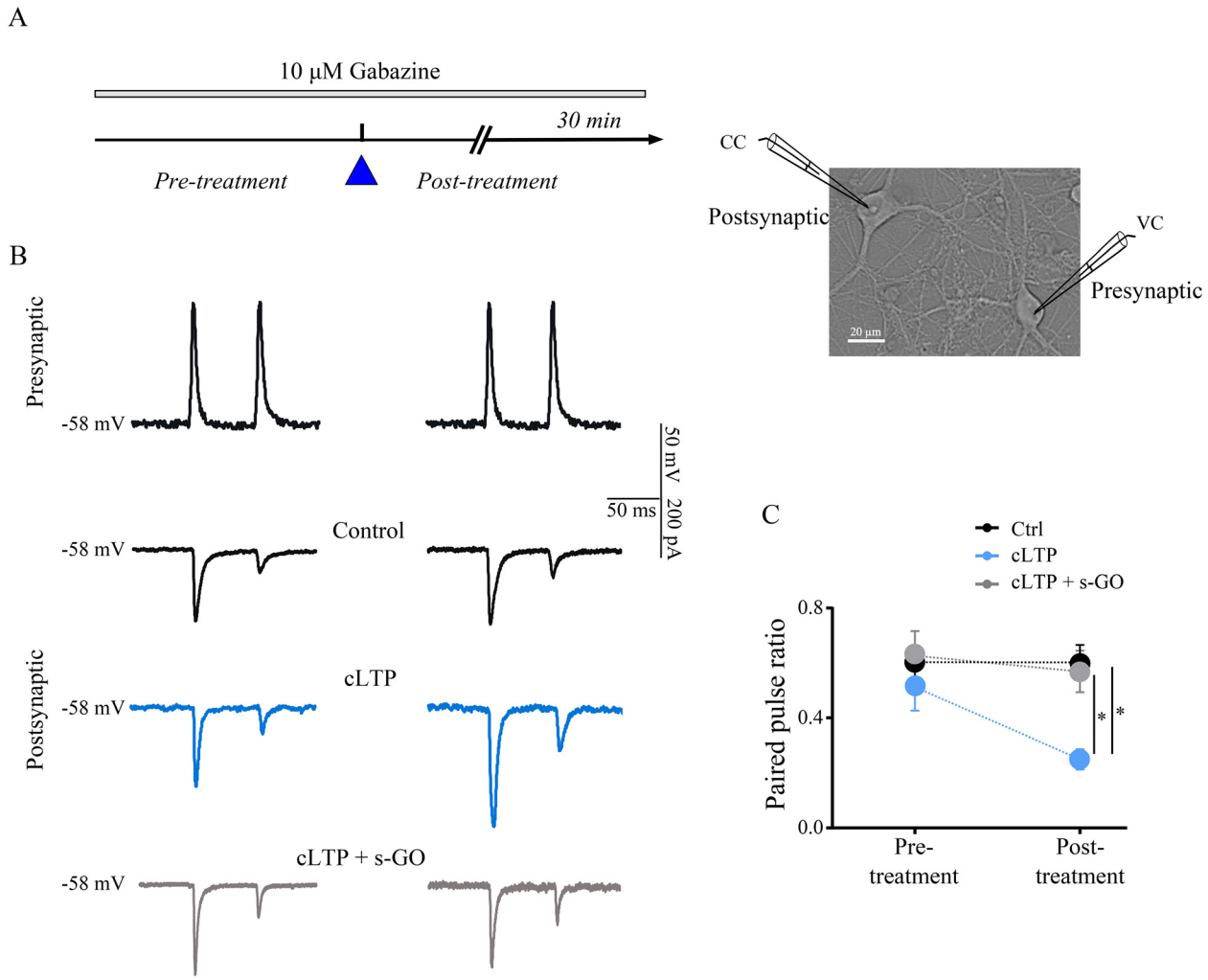

Fig. 4 s-GO reduces the probability of glutamate release in potentiated amygdala excitatory neurons. (A) Schematic representation (left) of the experimental protocol and bright field image (right) of simultaneous pair recordings of amygdala neurons. (B) Example tracings from pair recordings: top traces represent presynaptic action potentials while bottom ones represent the corresponding eEPSC prior (left) and after (24 min, right) treatment with saline (control, black traces), glutamate (cLTP, blue traces) or glutamate + s-GO (cLTP + s-GO, grey traces). (C) The plot summarizes the averaged paired-pulse ratio measured prior and after (24 min) each treatment. These were respectively 0.60 ± 0.06 and 0.60 ± 0.06 in control, 0.51 ± 0.09 and 0.25 ± 0.04 for cLTP and 0.62 ± 0.09 and 0.57 ± 0.07 for cLTP + s-GO; *$p < 0.05$.

enhanced and reduced p_r, respectively.[41,42] As shown in Fig. 4B, in control pairs (black traces) consecutive eEPSCs displayed short-term depression with no changes in PPR values prior and after saline treatment (n = 6 pairs; Fig. 4C). Differently, cells undergone to cLTP (in light blue, Fig. 4B), showed after the treatment a lower PPR (n = 8 pairs; Fig. 4C). In cLTP with s-GO (in grey, Fig. 4B), PPR, similarly to controls, was not affected by treatment (n = 6 pairs; Fig. 4C).

s-GO alone in control neurons reduced eEPSC peak amplitude[9] (ESI Fig. 4C†) and accordingly the PPR was increased (n = 6 pairs; ESI Fig. 4C and D†) to return within control values during washout (ESI Fig. 5†). These results were in agreement with the FM1-43 experiments and convincingly support the proposed mechanism of LTP block by s-GO nanosheets by reducing presynaptic vesicle re-cycling that lower p_r to block LTP-induced synaptic changes. Indeed, factors that modulate the release probability can favor or not synaptic LTP reinforcement.[38] We speculate that similarly *in vivo*, LTP triggered by the stressful event is impaired by s-GO *via* vesicle depletion and interruption. Despite being transient, this mechanism ultimately is able to prevent long-term dysfunctional plasticity and long-lasting anxiety behaviour.

3. Discussion

Our primary finding in this work is that the particular s-GO nanosheets that we have reported on previously, with a very consistent and reproducible structural and surface character, *via* inducing a transient decline in vesicle release in amygdala glutamatergic synapses, prevented the build-up of (dysfunctional) LTP and interrupted the vicious circle between the

stressful event and the development of long-lasting PTSD, without long-term effects on the homeostasis of non-potentiated synapses' function.

In the PTSD animal model used[11,18,43] the correlation between LA glutamatergic neuron hyperactivity and the emergence of anxiety behavior is widely accepted.[17,44] In a previous work[11] we have adopted this PTSD paradigm to challenge s-GO ability to downregulate *in vivo* glutamatergic synaptic activity.[9,10] This reduced the contextual fear response to the aversive stimulus (head out behavior)[45] and downregulated such a behavior, together with anxiety up to 48 hours from s-GO injection, a time frame where s-GO has been still detected in the injected brain tissue, and reported to reduce glutamatergic current frequency.[9]

In the current experiments, we show that in the same PTSD animal model, 4 days from injection, s-GO treatment reversed long-term contextual fear memory (head out) and long-lasting anxiety (EPM) behaviors, counteracting key steps of dysfunctional LTP which outlasted the nanosheets clearance.[9] We assessed the correct localization of the injecting cannula and the absence of general (*i.e.* motor) alterations ruling out potential s-GO nonspecific effects, confirming previous reports.[11] We propose that s-GO blocks crucial processes in the reinforcement of dysfunctional LTP, needed to develop altered behavior in this PTSD model, a hypothesis supported by LA dendritic spine measures[46] when comparing WC animals with or without s-GO treatment. In addition, dendritic spines were not affected by s-GO treatment in the absence of fear memory consolidation (UC animals), suggesting this effect be restricted to upstream LTP-driven spine dynamics.

Regarding the subcellular interaction of the nanomaterial with neurons, GO, *via* adhesion to the plasma membrane, may alter the mechanical features of the lipid bilayer[47] and perturb membrane dynamics or lipids exchange.[48] As speculated in our previous work,[9] the specific targeting of excitatory neurons might be related to the particular range of s-GO lateral dimension, compatible with the size and organization of glutamatergic synapses.[49] In fact, larger or smaller GO flakes did not modulate glutamate-mediated synaptic transmission.[9]

Our *in vitro* findings provide direct support for s-GO interference with the presynaptic site of glutamatergic synapses to account for its influence in amygdala (pathological) plasticity. In amygdala cultured neurons, cLTP induction[11] resulted in an increase in pre- and post-synaptic markers of glutamatergic synapses and in their co-localization, indicative of augmented excitatory functional connections. These results are in agreement with studies on amygdala acute slices obtained from animals undergone to Pavlovian fear conditioning, showing the involvement of both pre- and post-synaptic factors in LTP expression of LA.[50,51] The potentiation in glutamatergic markers is in agreement with the long-term enhancement in mEPSCs amplitude and frequency observed following cLTP, in fact frequency and amplitude of miniatures are accepted reporters of changes in pre and postsynaptic features of CNS synapses.[29] The late onset of mEPSCs frequency increase might depend on modifications of the presynaptic site occurring at a later stage, as reported for example in the hippocampus, where pre and postsynaptic components of LTP might be temporally distinct.[52] Morphological and functional changes due to cLTP were efficiently blocked by s-GO *in vitro*, apparently due to a reduction in the p_r, as supported by FM1-43 measures. Although not selective for glutamatergic vesicles, these experiments reveal the ability of the 2D nanosheets to revert to baseline levels the kinetics of vesicles unloading in putative pyramidal cells[37] undergone to cLTP.

s-GO modulation of the p_r is well suited to down-regulate LTP and this effect was further strengthened by paired pulse experiments, a classical paradigm to assess the p_r of the readily releasable vesicle pool at central synapses.[53] In dual recordings from mono-synaptically connected excitatory neurons, s-GO reduced the amplitude of the first eEPSC and increased the PPR when applied alone or in the presence of cLTP, both events indicative of a decrease in the p_r.[41,42] Thus, several factors make the s-GO transient regulation of recyclable vesicle dynamics effective at impairing LTP. Our study excludes a direct chemical interaction between s-GO and glutamate or between s-GO and glutamate post-synaptic receptors.

4. Conclusions

Despite the extensive research and recent advances in understanding the neurobiological systems implicated in PTSD development,[54] only 30% of treatments achieve full remission of this disabling condition.[55] Our results, in addition to the potential exploitation of the specific s-GO nanosheets as a delivery platform,[56,57] indicate in glutamate vesicle recycling a downstream molecular mechanism underpinning amygdala plasticity which can be the target of future nanotechnology-based treatments. The potential of such approaches is also corroborated by the GO safety in the interaction with the blood–brain barrier,[58] supporting the feasibility of other less invasive routes of administration, alternative to the intrathecal one used in this work. Our PTSD model, using a stressor cue in a classical contextual fear conditioning paradigm, focuses on synaptic changes in the amygdala assuming their implication in PTSD[59] with the potential of the design of novel treatments. Indeed, abnormal synaptic plasticity and neurotransmitter imbalances in the amygdaloid complex that affect the processing and regulation of emotions, contributing to the pathophysiology of PTSD, were observed in both predator-stress animal model and human studies. However, it is important to note that the long-lasting increase in the fear memory observed in such a model gradually weakens over time together with the anxiety.

5. Materials and methods

5.1 Graphene oxide nanosheets synthesis and characterization

The s-GO material used in these studies has been synthesized according to the protocols that have already been reported and

characterized extensively in our previous published work.[11] See ESI† for further details.

5.2 The *in vivo* PTSD model and design of treatments

Experimental procedures were carried out in accordance with the Italian law (decree 26/14) and the EU guidelines (2007/526/CE and 2010/63/UE) and were approved by the Italian Ministry of Health (no. 22DAB.11). See ESI† for further details.

5.3 Golgi-Cox staining and dendritic spine analysis

See ESI.†

***In vitro* dissociated amygdala cultures.** All experimental procedures were performed in agreement with the Italian law (decree 26/14) and the European Union (EU) guidelines (2007/526/CE and 2010/63/UE) and were authorized by the Italian Ministry of Health (no. 689/2017-PR, no. 22DAB.N.1Z8 and no. 22DAB.N.1WO). The animal handling was approved by the local veterinary authorities and by the institutional (SISSA) ethical committee.

Primary cultures of amygdala cells were obtained from postnatal (P7–10) juvenile Wistar rats and prepared as previously described[11] with slight modifications. See ESI† for further details.

5.4 Immunohistochemistry and confocal microscopy

See ESI.†

5.5 Electrophysiology

Patch clamp whole-cell recordings were obtained from dissociated amygdala neurons using glass micropipettes with a resistance of 4–7 MΩ once filled with the following intracellular saline solution (in mM): 120 K gluconate, 20 KCl, 10 HEPES, 10 EGTA, 2 $MgCl_2$, 2 Na_2ATP (pH 7.3, osmolarity adjusted to 300 mOsm). All experiments were performed at RT with the standard extracellular solution containing (in mM) 150 NaCl, 4 KCl, 2 $CaCl_2$, 1 $MgCl_2$, 10 HEPES, 10 glucose (pH 7.4) and continuously perfused at 2 mL min^{-1}. All data were collected by means of a Multiclamp 700A patch amplifier (Axon CNS, Molecular Devices) and digitized at 10 kHz with the pClamp 10.6 acquisition-software (Molecular Devices LLC, USA). See ESI† for further details.

5.6 FM1-43 imaging

See ESI.†

5.7 Data analysis and statistics

All values from samples subjected to the same experimental protocols were pooled together and expressed as mean ± s.e.m. with n = number of cells, unless otherwise indicated. For *in vivo* experiments, data from independent groups of animals were checked for normality and homogeneity and analyzed using Student's unpaired two-tailed t-test. All comparisons between two independent variables were made with two-way ANOVAs, followed by Bonferroni or Tukey' multiple comparison test when appropriated. For electrophysiological data, Shapiro–Wilk normality test was applied to evaluate the statistical distribution of the data sets. Statistically significant difference between two data sets was assessed by Student's t-test for parametric data and by Mann–Whitney for non-parametric ones. All comparisons between more than 2 groups were made with one-way ANOVA for parametric data, followed by using Holm–Sidak's multiple comparisons test for *post hoc* analysis. Not parametric data were analyzed with Kruskal–Wallis test and *post hoc* analysis was done with Dunn's multiple comparison test. Statistical significance was determined at $P < 0.05$, unless otherwise indicated.

Data availability

All the data that support the findings of this study are available within the article and in its ESI,† and these data are available from the corresponding author on request.

Author contributions

The manuscript was written through contributions of all authors. All authors have given approval to the final version of the manuscript. EP and GC performed all *in vitro* experiments and analysis; AFB and RC performed all *in vivo* experiments and analysis; NL and KK perform and design the s-GO experimental strategy; KK, GC and LB conceived the study; GC and LB designed the experimental plan, interpreted the results and wrote the manuscript.

Conflicts of interest

There are no conflicts to declare.

Acknowledgements

This work received funding from the European Union Horizon 2020 Research and Innovation Programme under Grant Agreement No. GrapheneCore3 (881603). We would like to acknowledge Dr Michelle Ntola for contributions in the synthesis of s-GO materials and Dr M. Arellano and Ms A. Karakasidi for their contributions with the GO characterization. The ICN2 is funded by the CERCA programme/Generalitat de Catalunya and has been supported by the Severo Ochoa Centres of Excellence programme [SEV-2017-0706] and is currently supported by the Severo Ochoa Centres of Excellence programme, grant CEX2021-001214-S, both funded by MCIN/AEI/10.13039.501100011033.

References

1 A. K. Geim and K. S. Novoselov, The rise of graphene, *Nat. Mater.*, 2007, **6**, 183–191.

2 A. Garcia-Etxarri and R. Yuste, Time for NanoNeuro, *Nat. Methods*, 2021, **18**, 1287–1293.
3 E. K. Drexler, C. Peterson and G. Pergamit, *Unbounding the Future: The Nanotechnology Revolution*, William Morrow and Company, Inc., New York, NY, USA, 1st edn, 1991.
4 S. Bayda, M. Adeel, T. Tuccinardi, M. Cordani and F. Rizzolio, The History of Nanoscience and Nanotechnology: From Chemical–Physical Applications to Nanomedicine, *Molecules*, 2020, **25**, 112.
5 L. Feng, L. Wu and X. Qu, New horizons for diagnostics and therapeutic applications of graphene and graphene oxide, *Adv. Mater.*, 2013, **25**, 168–186.
6 K. Kostarelos, M. Vincent, C. Hebert and J. A. Garrido, Graphene in the Design and Engineering of Next-Generation Neural Interfaces, *Adv. Mater.*, 2017, **29**, 1700909.
7 M. Bramini, G. Alberini, E. Colombo, M. Chiacchiaretta, M. L. DiFrancesco, J. F. Maya-Vetencourt, L. Maragliano, F. Benfenati and F. Cesca, Interfacing Graphene-Based Materials With Neural Cells, *Front. Syst. Neurosci.*, 2018, **12**, 12.
8 G. Cellot, A. Franceschi Biagioni and L. Ballerini, Nanomedicine and graphene-based materials: advanced technologies for potential treatments of diseases in the developing nervous system, *Pediatr. Res.*, 2022, **92**, 71–79.
9 R. Rauti, M. Medelin, L. Newman, S. Vranic, G. Reina, A. Bianco, M. Prato, K. Kostarelos and L. Ballerini, Graphene Oxide Flakes Tune Excitatory Neurotransmission *in Vivo* by Targeting Hippocampal Synapses, *Nano Lett.*, 2019, **19**, 2858–2870.
10 G. Cellot, S. Vranic, Y. Shin, R. Worsley, A. F. Rodrigues, C. Bussy, C. Casiraghi, K. Kostarelos and J. R. McDearmid, Graphene oxide nanosheets modulate spinal glutamatergic transmission and modify locomotor behaviour in an *in vivo* zebrafish model, *Nanoscale Horiz.*, 2020, **5**, 1250–1263.
11 A. Franceschi Biagioni, G. Cellot, E. Pati, N. Lozano, B. Ballesteros, R. Casani, N. C. Coimbra, K. Kostarelos and L. Ballerini, Graphene oxide prevents lateral amygdala dysfunctional synaptic plasticity and reverts long lasting anxiety behavior in rats, *Biomaterials*, 2021, **271**, 120749.
12 L. M. Shin and I. Liberzon, The neurocircuitry of fear, stress, and anxiety disorders, *Neuropsychopharmacology*, 2010, **35**, 169–191.
13 D. M. Bannerman, R. Sprengel, D. J. Sanderson, S. B. McHugh, J. N. Rawlins, H. Monyer and P. H. Seeburg, Hippocampal synaptic plasticity, spatial memory and anxiety, *Nat. Rev. Neurosci.*, 2014, **15**, 181–192.
14 M. P. Parsons and L. A. Raymond, Extrasynaptic NMDA receptor involvement in central nervous system disorders, *Neuron*, 2014, **82**, 279–293.
15 L. H. Somerville, H. Kim, T. Johnstone, A. L. Alexander and P. J. Whalen, Human amygdala responses during presentation of happy and neutral faces: correlations with state anxiety, *Biol. Psychiatry*, 2004, **55**, 897–903.
16 M. L. Pacella, B. Hruska and D. L. Delahanty, The physical health consequences of PTSD and PTSD symptoms: a meta-analytic review, *J. Anxiety Disord.*, 2013, **27**, 33–46.
17 J. A. Rosenkranz, E. R. Venheim and M. Padival, Chronic stress causes amygdala hyperexcitability in rodents, *Biol. Psychiatry*, 2010, **67**, 1128–1136.
18 R. A. Dielenberg, G. E. Hunt and I. S. McGregor, "When a rat smells a cat": the distribution of Fos immunoreactivity in rat brain following exposure to a predatory odor, *Neuroscience*, 2001, **104**, 1085–1097.
19 C. Muñoz-Abellán, N. Daviu, C. Rabasa, R. Nadal and A. Armario, Cat odor causes long-lasting contextual fear conditioning and increased pituitary-adrenal activation, without modifying anxiety, *Horm. Behav.*, 2009, **56**, 465–471.
20 A. F. Rodrigues, L. Newman, N. Lozano, S. P. Mukherjee, B. Fadeel, C. Bussy and K. Kostarelos, A Blueprint for the Synthesis and Characterisation of Thin Graphene Oxide with Controlled Lateral Dimensions for Biomedicine, *2D Mater.*, 2018, **5**, 035020.
21 N. C. Coimbra, T. Paschoalin-Maurin, G. S. Bassi, A. Kanashiro, A. F. Biagioni, T. T. Felippotti, *et al.*, Critical neuropsychobiological analysis of panic attack-and anticipatory anxiety-like behaviors in rodents confronted with snakes in polygonal arenas and complex labyrinths: a comparison to the elevated plus- and T-maze behavioral tests, *Braz. J. Psychiat.*, 2017, **39**, 72–83.
22 D. I. Choi, J. Kim, H. Lee, J. Kim, Y. Sung, J. E. Choi, S. J. Venkat, P. Park, H. Jung and B.-K. Kaang, Synaptic correlates of associative fear memory in the lateral amygdala, *Neuron*, 2021, **109**, 2717–2726.e3.
23 P. Chakraborty and S. Chattarji, Timing is everything: differential effects of chronic stress on fear extinction, *Psychopharmacology*, 2019, **236**, 73–86.
24 R. Mitra, R. Adamec and R. Sapolsky, Resilience against predator stress and dendritic morphology of amygdala neurons, *Behav. Brain Res.*, 2009, **205**, 535–543.
25 N. P. Pampaloni, M. Lottner, M. Giugliano, A. Matruglio, F. D'Amico, M. Prato, J. A. Garrido, L. Ballerini and D. Scaini, Single-layer graphene modulates neuronal communication and augments membrane ion currents, *Nat. Nanotechnol.*, 2018, **13**, 755–764.
26 K. S. Yoo, K. Lee, J. Y. Oh, H. Lee, H. Park, Y. S. Park and H. K. Kim, Postsynaptic density protein 95 (PSD-95) is transported by KIF5 to dendritic regions, *Mol. Brain*, 2019, **12**, 97.
27 M. Borczyk, M. A. Śliwińska, A. Caly, *et al.*, Neuronal plasticity affects correlation between the size of dendritic spine and its postsynaptic density, *Sci. Rep.*, 2019, **9**, 1693.
28 F. McLeod, A. Marzo, M. Podpolny, S. Galli and P. Salinas, Evaluation of Synapse Density in Hippocampal Rodent Brain Slices, *J. Visualized Exp.*, 2017, **128**, 56153.
29 V. V. Uteshev and P. S. Pennefather, A mathematical description of miniature postsynaptic current generation at central nervous system synapses, *Biophys. J.*, 1996, **71**, 1256–1266.
30 A. Malgaroli and R. W. Tsien, Glutamate-induced long-term potentiation of the frequency of miniature synaptic cur-

rents in cultured hippocampal neurons, *Nature*, 1992, **357**, 134–139.
31 R. J. Cormier, M. D. Mauk and P. T. Kelly, Glutamate iontophoresis induces long-term potentiation in the absence of evoked presynaptic activity, *Neuron*, 1993, **10**, 907–919.
32 M. A. Gaffield and W. J. Betz, Imaging synaptic vesicle exocytosis and endocytosis with FM dyes, *Nat. Protoc.*, 2006, **1**, 2916–2921.
33 W. J. Betz and G. S. Bewick, Optical Analysis of Synaptic Vesicle Recycling at the Frog Neuromuscular Junction, *Science*, 1992, **255**(5041), 200–203.
34 T. A. Ryan, H. Reuter, B. Wendland, F. E. Schweizer, R. W. Tsien and S. J. Smith, The Kinetics of Synaptic Vesicle Recycling Measured at Single Presynaptic Boutons, *Neuron*, 1993, **11**, 713–724.
35 P. Verstreken, T. Ohyama and H. J. Bellen, FM 1-43 Labeling of synaptic vesicle pools at the Drosophila neuromuscular junction, *Methods Mol. Biol.*, 2008, **440**, 349–369.
36 S. S. Zakharenko, L. Zablow and S. A. Siegelbaum, Visualization of changes in presynaptic function during long-term synaptic plasticity, *Nat. Neurosci.*, 2001, **4**, 711–717.
37 D. G. Rainnie, E. K. Asprodini and P. Shinnick-Gallagher, Intracellular recordings from morphologically identified neurons of the basolateral amygdala, *J. Neurophysiol.*, 1993, **69**, 1350–1362.
38 S. Gasparini, C. Saviane, L. L. Voronin and E. Cherubini, Silent synapses in the developing hippocampus: lack of functional AMPA receptors or low probability of glutamate release?, *Proc. Natl. Acad. Sci. U. S. A.*, 2000, **97**, 9741–9746.
39 V. N. Murthy, T. J. Sejnowski and C. F. Stevens, Heterogeneous release properties of visualized individual hippocampal synapses, *Neuron*, 1997, **18**, 599–612.
40 R. S. Zucker, Short-term synaptic plasticity, *Annu. Rev. Neurosci.*, 1989, **12**, 13–31.
41 D. Debanne, N. C. Guérineau, B. H. Gähwiler and S. M. Thompson, Paired-pulse facilitation and depression at unitary synapses in rat hippocampus: quantal fluctuation affects subsequent release, *J. Physiol.*, 1996, **491**, 163–176.
42 T. Manabe, D. J. Wyllie, D. J. Perkel and R. A. Nicoll, Modulation of synaptic transmission and long-term potentiation: effects on paired pulse facilitation and EPSC variance in the CA1 region of the hippocampus, *J. Neurophysiol.*, 1993, **70**, 1451–1459.
43 L. K. Takahashi, B. R. Nakashima, H. Hong and K. Watanabe, The smell of danger: a behavioral and neural analysis of predator odor-induced fear, *Neurosci. Biobehav. Rev.*, 2005, **29**, 1157–1167.
44 H. T. Blair, G. E. Schafe, E. P. Bauer, S. M. Rodrigues and J. E. LeDoux, Synaptic Plasticity in the Lateral Amygdala: A Cellular Hypothesis of Fear Conditioning, *Learn. Mem.*, 2001, **8**, 229–242.
45 I. McGregor, L. Schrama, P. Ambermoon and R. A. Dielenberg, Not all 'predator odours' are equal: cat odour but not 2,4,5 trimethylthiazoline (TMT; fox odour) elicits specific defensive behaviours in rats, *Behav. Brain Res.*, 2002, **129**, 1–16.
46 M. Bosch, J. Castro, T. Saneyoshi, H. Matsuno, M. Sur and Y. Hayashi, Structural and molecular remodeling of dendritic spine substructures during long-term potentiation, *Neuron*, 2014, **82**, 444–459.
47 Z. Song, Y. Wang and Z. Xu, Mechanical responses of the bio-nano interface: A molecular dynamics study of graphene-coated lipid membrane, *Theor. Appl. Mech. Lett.*, 2015, **5**, 231–235.
48 S. P. Mukherjee, B. Lazzaretto, K. Hultenby, L. Newman, A. F. Rodrigues, N. Lozano, K. Kostarelos, P. Malmberg and B. Fadeel, Graphene Oxide Elicits Membrane Lipid Changes and Neutrophil Extracellular Trap Formation, *Chem*, 2018, **4**, 334–358.
49 B. High, A. A. Cole, X. Chen and T. S. Reese, Electron microscopic tomography reveals discrete transcleft elements at excitatory and inhibitory synapses, *Front. Synaptic Neurosci.*, 2015, **7**, 9.
50 S. Maren, Synaptic mechanisms of associative memory in the amygdala, *Neuron*, 2005, **47**, 783–786.
51 S. Rumpel, J. LeDoux, A. Zador and R. Malinow, Postsynaptic receptor trafficking underlying a form of associative learning, *Science*, 2005, **308**, 83–88.
52 I. T. Bayazitov, R. J. Richardson, R. G. Fricke and S. S. Zakharenko, Slow presynaptic and fast postsynaptic components of compound long-term potentiation, *J. Neurosci.*, 2007, **27**, 11510–11521.
53 L. E. Dobrunz and C. F. Stevens, Heterogeneity of release probability, facilitation, and depletion at central synapses, *Neuron*, 1997, **18**, 995–1008.
54 A. L. Mahan and K. J. Ressler, Fear conditioning, synaptic plasticity and the amygdala: implications for posttraumatic stress disorder, *Trends Neurosci.*, 2012, **35**, 24–35.
55 B. Kelmendi, T. G. Adams, S. Yarnell, S. Southwick, C. G. Abdallah and J. H. Krystal, PTSD: from neurobiology to pharmacological treatments, *Eur. J. Psychotraumatology*, 2016, **7**, 31858.
56 G. Cellot, A. Franceschi Biagioni and L. Ballerini, Nanomedicine and graphene-based materials: advanced technologies for potential treatments of diseases in the developing nervous system, *Pediatr. Res.*, 2022, **92**, 71–79.
57 A. M. L. Oliveira, M. Machado, G. A. Silva, D. B. Bitoque, J. Tavares Ferreira, L. Abegão Pinto and Q. Ferreira, Graphene oxide thin films with drug delivery function, *Nanomaterials*, 2022, **12**, 1149.
58 V. Castagnola, L. Deleye, A. Podestà, E. Jaho, F. Loiacono, D. Debellis, M. Trevisani, D. Z. Ciobanu, A. Armirotti, F. Pisani, E. Flahaut, E. Vazquez, M. Bramini, F. Cesca and F. Benfenati, Interactions of Graphene Oxide and Few-Layer Graphene with the Blood–Brain Barrier, *Nano Lett.*, 2023, **23**, 2981–2990.
59 T. C. M. Bienvenu, C. Dejean, D. Jercog, B. Aouizerate, M. Lemoine and C. Herry, The advent of fear conditioning as an animal model of post-traumatic stress disorder: Learning from the past to shape the future of PTSD research, *Neuron*, 2021, **109**, 2380–2397.